

# An Integration Algorithm for Stator Flux Estimation of a Direct-Torque-Controlled Electrical Excitation Flux-Switching Generator

Yu Wang, *Associate Member, IEEE*, and Zhiqian Deng

**Abstract**—This paper presents an integration algorithm for stator flux estimation of direct torque control (DTC). This algorithm only contains a fifth-order low-pass filter (LPF), a high-pass (HP) filter, and a simple logical calculation part, where the fifth-order LPF and the HP filter can effectively filter out HF harmonics and the dc drift in the back EMF, respectively. The  $\alpha$ - and  $\beta$ -axis back EMFs passing through the two filters will obtain  $\beta$ -axis stator flux linkage and opposite polarity  $\alpha$ -axis stator flux linkage, respectively, and then by the logical calculation part can finally achieve  $\alpha$ - and  $\beta$ -axis stator flux linkages. At any synchronous angular frequency, the amplitude- and phase-frequency characteristics of this algorithm are same as those of the pure integrator, and meanwhile its dc gain is zero. The proposed algorithm with high estimation accuracy behaves well in both steady state and dynamic performance when used in a DTC-based electrical excitation flux-switching generator dc power system, which is verified by experimental results.

**Index Terms**—Direct torque control (DTC), electrical excitation flux-switching (EEFS) generator, integration algorithm, stator flux estimation.

## I. INTRODUCTION

IN most high-performance brushless ac (BLAC) machine drives including those based on direct torque control (DTC) and field-oriented control, one of the critical tasks is stator flux estimation [1]–[4]. The estimation accuracy of the stator flux will affect not only the stability and quality of the control schemes, but also steady state and dynamic performance of the system [5].

The voltage model is a convenient stator flux estimator due to its simplicity. However, it is well known that pure integrators suffer from two major problems [6], [7].

- 1) DC drift because a dc component is always present in the signal to be processed, thus, leading the integrator to saturation.

Manuscript received August 7, 2011; revised November 5, 2011 and January 5, 2012; accepted February 4, 2012. Date of publication March 13, 2012; date of current version May 18, 2012. This work was supported by the Aviation Science funds of China under Project 2009ZB52025, the Postgraduate Research and Innovation Project of University in Jiangsu Province under Project CX08B\_068Z, and the Research Fund for the Doctoral Program of Higher Education of China under Project 20113218130001. Paper no. TEC-00409-2011.

The authors are with the Department of Electrical Engineering, Nanjing University of Aeronautics and Astronautics, Nanjing, 210016 China (e-mail: yuwang0125@yahoo.com.cn; dzq@nuaa.edu.cn).

Color versions of one or more of the figures in this paper are available online at <http://ieeexplore.ieee.org>.

Digital Object Identifier 10.1109/TEC.2012.2188139

- 2) Initial conditions, which lead to the appearance of a dc drift at the output of the integrator, which actually does not exist.

Attempts have been made to modify the pure integrator by implementing it applying a low-pass filter (LPF) [8], [9]. LPF will produce errors in magnitude and phase angle especially if the excitation frequency is lower than the cutoff frequency of the LPF [10]. Several improved estimation methods have been investigated [7], [11]–[13]. In [7], a feedback block is added after the LPF and transformation parts between Cartesian to polar coordinates are introduced, which can improve the estimation performance. The proposed method used an adaptive control system, which was based on the fact that the back EMF is orthogonal to the stator flux. The compensator is adapted for this condition. Cirrincione *et al.* [11] propose an adaptive notch filter for the elimination of the dc component in the integration of signals used for the flux estimation in high-performance ac drives. This integration method is composed of two identical adaptive noise cancellers using a linear neural network with just one bias weight. In [12], a pure integrator is employed for stator flux estimation, which permits high-estimation bandwidth. Compensation of the drift components is done by offset identification. The nonlinear voltage distortions are corrected by a self-adjusting inverter model. In [13], the time-variable dc offset voltage is estimated from the flux drift in a parallel stator model and used to eliminate the offset by feedforward control. Residual HF disturbances are compensated by feedback flux amplitude control.

In order to improve flux estimation accuracy and reduce system complexity, a simple integration algorithm for stator flux estimation is proposed in this paper. This algorithm consists of a fifth-order LPF, a high-pass (HP) filter, and a logical calculation part, which can effectively solve the problems the pure integrator generated and will not bring errors both in magnitude and phase angle. Furthermore, the dc gain of this method is zero, thus, dc offset errors will be eliminated completely. The proposed algorithm is applied in a DTC-based electrical excitation flux-switching (EEFS) generator dc power system. As a novel brushless ac machine, the EEFS machine exhibits advantages including double salient structure, bipolar and sinusoidal flux linkage, and good flux regulation capability, and thus is suitable for use as a generator in dc power systems.

This paper is organized as follows. The electromagnetic performance of the EEFS machine and its DTC scheme are described in Section II. Section III describes and discusses the proposed algorithm. The performance of the proposed



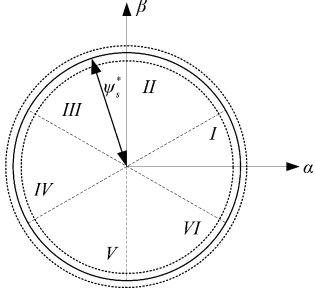


Fig. 4. Stator flux-linkage sectors.

TABLE I  
SWITCH TABLE FOR THE DTC SCHEME

$\psi$	$\tau$	$\theta_k$					
		I	II	III	IV	V	VI
1	1	V2	V3	V4	V5	V6	V1
	0	V0	V0	V0	V0	V0	V0
-1	1	V3	V4	V5	V6	V1	V2
	0	V0	V0	V0	V0	V0	V0

### III. INTEGRATION ALGORITHM FOR STATOR FLUX ESTIMATION

As mentioned previously, both the pure integrator and the LPF have application problems when they are used for flux estimation [6], [7]. Therefore, in order to obtain  $\psi_{s\alpha}$  and  $\psi_{s\beta}$  without errors in phase angle and magnitude, series filters, which can produce the required lag phase angle, are needed and deduced as follows.

The  $\alpha$ - and  $\beta$ -axis stator flux linkages ( $\psi_{s\alpha}$  and  $\psi_{s\beta}$ ) are lag  $90^\circ$  behind the  $\alpha$ - and  $\beta$ -axis back EMFs ( $-e_\alpha$  and  $-e_\beta$ ), respectively, which can be consider as  $\psi_{s\beta}$  is lag  $180^\circ$  behind  $-e_\alpha$  and  $\psi_{s\alpha}$  is lag  $180^\circ$  behind  $-e_\beta$ .

An LPF ( $\sqrt{2}\omega_e/s + \omega_e$ ) is applied primarily, when  $\omega_e = \omega_1$  ( $\omega_1$  is the synchronous angular frequency of the machine), the produced lag phase angle is  $45^\circ$ , hence, at least four  $\sqrt{2}\omega_e/s + \omega_e$  components are required to reach  $180^\circ$ , i.e.,  $(\sqrt{2}\omega_1/s + \omega_1)^4 (1/\omega_1)$  is required, where  $1/\omega_1$  means that the magnitude of the stator flux linkage is  $1/\omega_1$  of that of the back EMF. However, the dc gain of  $(\sqrt{2}\omega_1/s + \omega_1)^4 (1/\omega_1)$  is not zero; thus, a  $\sqrt{2}s/s + \omega_1$  part is needed and a  $\sqrt{2}\omega_1/s + \omega_1$  part is also required to compensate the forward phase angle produced by  $\sqrt{2}s/s + \omega_1$  part. Therefore, the following series filter can be obtained:

$$\begin{aligned} & \left( \frac{\sqrt{2}\omega_1}{s + \omega_1} \right)^5 \frac{\sqrt{2}s}{s + \omega_1} \frac{1}{\omega_1} \\ &= \frac{4\sqrt{2}\omega_1^4}{s^5 + 5\omega_1 s^4 + 10\omega_1^2 s^3 + 10\omega_1^3 s^2 + 5\omega_1^4 s + \omega_1^5} \frac{\sqrt{2}s}{s + \omega_1}. \end{aligned} \quad (2)$$

Hence, an integration algorithm based on the fifth-order LPF is proposed, as shown in Fig. 5. This algorithm contains a fifth-order LPF, an HP filter, and a logical calculation part.

In Fig. 5, at  $\omega_1$ , the amplitude- and phase-frequency characteristics as well as the dc gain of the fifth-order LPF are as follows:

$$H_{LP}(j\omega_1) = \frac{1}{\omega_1} \quad (3)$$

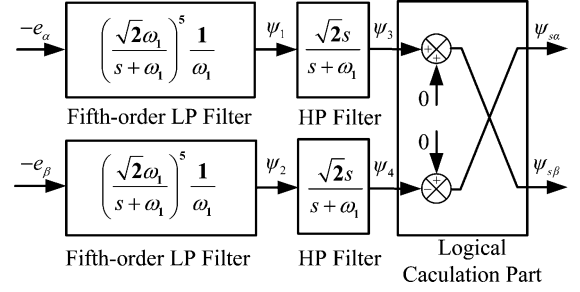


Fig. 5. Block diagram of the integration algorithm.

$$\angle H_{LP}(j\omega_1) = -225^\circ \quad (4)$$

$$H_{LP}(j0) = \frac{4\sqrt{2}}{\omega_1}. \quad (5)$$

The  $\alpha$ - and  $\beta$ -axis back EMFs are expressed as follows:

$$-e_\alpha = E \cos(\omega_1 t + \delta) + U_{d\alpha} \quad (6)$$

$$-e_\beta = E \cos(\omega_1 t + \delta - 90^\circ) + U_{d\beta} \quad (7)$$

where  $U_{d\alpha}$ ,  $U_{d\beta}$  are the dc offset components.

Then, the outputs of the fifth-order LPF can be yield by:

$$\psi_1 = \frac{E}{\omega_1} \cos(\omega_1 t + \delta - 225^\circ) + \frac{4\sqrt{2}}{\omega_1} U_{d\alpha} \quad (8)$$

$$\psi_2 = \frac{E}{\omega_1} \cos(\omega_1 t + \delta - 315^\circ) + \frac{4\sqrt{2}}{\omega_1} U_{d\beta}. \quad (9)$$

The amplitude- and phase-frequency characteristics as well as the dc gain of the HP filter are as follows:

$$H_{HP}(j\omega_1) = 1 \quad (10)$$

$$\angle H_{HP}(j\omega_1) = 45^\circ \quad (11)$$

$$H_{HP}(j0) = 0. \quad (12)$$

Hence, the outputs of the HP filter can be expressed as follows:

$$\psi_3 = \frac{E}{\omega_1} \cos(\omega_1 t + \delta - 180^\circ) = \psi_{s\beta} \quad (13)$$

$$\begin{aligned} \psi_4 &= \frac{E}{\omega_1} \cos(\omega_1 t + \delta - 270^\circ) \\ &= \frac{E}{\omega_1} \cos(\omega_1 t + \delta - 90^\circ - 180^\circ) \\ &= -\frac{E}{\omega_1} \cos(\omega_1 t + \delta - 90^\circ) = -\psi_{s\alpha} \end{aligned} \quad (14)$$

where  $\psi_{s\alpha}$  and  $\psi_{s\beta}$  are the  $\alpha$ - and  $\beta$ -axis stator flux linkages, respectively.

Therefore,  $\psi_{s\alpha}$  and  $\psi_{s\beta}$  can be obtained by the logical calculation part as follows:

$$\psi_{s\alpha} = 0 - \psi_4 \quad (15)$$

$$\psi_{s\beta} = 0 + \psi_3. \quad (16)$$

According to (2)–(16), Fig. 5 can be simplified to Fig. 6.

In Fig. 5, the HP filter in combination with the LPF can cancel the dc drift. At  $t = 0$ , if a dc drift ( $U_d * 1(t)$ ) acts on the series

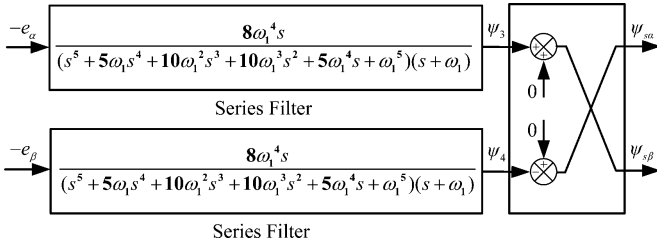


Fig. 6. Simplified block diagram of the integration algorithm.

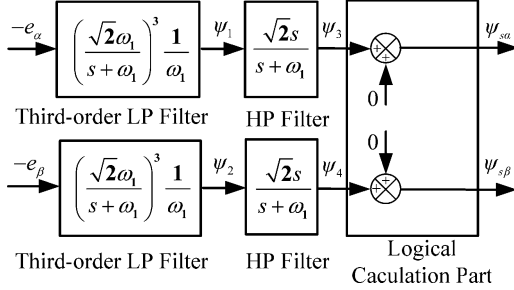


Fig. 7. Block diagram of the integration algorithm based on third-order LPF.

filter, according to the final value theorem, the final value of the output is as follows:

$$\lim_{t \rightarrow \infty} h(t) = \lim_{s \rightarrow 0} sH(s) = \lim_{s \rightarrow 0} s \frac{U_d}{s} \left( \frac{\sqrt{2}\omega_1}{s + \omega_1} \right)^5 \frac{1}{\omega_1} \frac{\sqrt{2}s}{s + \omega_1} = 0. \quad (17)$$

As can be seen, dc offsets in the back EMF can be completely filtered out by the HP filter.

Besides, another integration algorithm based on third-order LPF can also be obtained, as shown in Fig. 7.

Compared with the algorithm in Fig. 5, the algorithm in Fig. 7 is simpler and has a lower computer load.

However, when the machine operates at  $\omega_1$ , for high harmonics ( $\omega_n = n\omega_1$ ), the amplitude-frequency characteristics of the fifth-order LPF in Fig. 5, the third-order LPF in Fig. 7, and the pure integrator are as follows:

$$H_5(j\omega_n) = \frac{4\sqrt{2}}{(n^2 + 1)^{5/2} \omega_1} \quad (18)$$

$$H_3(j\omega_n) = \frac{2\sqrt{2}}{(n^2 + 1)^{3/2} \omega_1} \quad (19)$$

$$H(j\omega_n) = \frac{1}{n\omega_1} \quad (20)$$

when  $n \geq 2$ ,  $H_5(j\omega_n) < H_3(j\omega_n) < H(j\omega_n)$ .

Due to pulswidth modulation control and measurement noises, there is a large amount of harmonics in the back EMF, and the algorithm in Fig. 5 behaves better in filtering out the harmonics.

Furthermore, Table II compares the characteristics of the proposed algorithm, the pure integrator, and the LPF.

From Table II and the previous analysis, the advantages of the proposed integration algorithm can be concluded as follows.

TABLE II  
COMPARISON OF THE PROPOSED ALGORITHM, THE PURE INTEGRATOR, AND THE LPF

	The Proposed Algorithm	Pure Integrator( $\frac{1}{s}$ )	LPF( $\frac{1}{s + \omega_c}$ )
$H(j\omega)$	$1/ \omega $	$1/ \omega $	$1/\sqrt{\omega_c^2 + \omega^2}$
$\angle H(j\omega)$	$-90^\circ$	$-90^\circ$	$-\arctg \frac{\omega}{\omega_c}$
$H(j0)$	0	$\infty$	$1/ \omega_c $

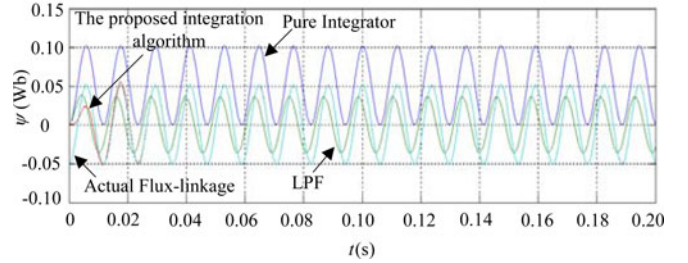
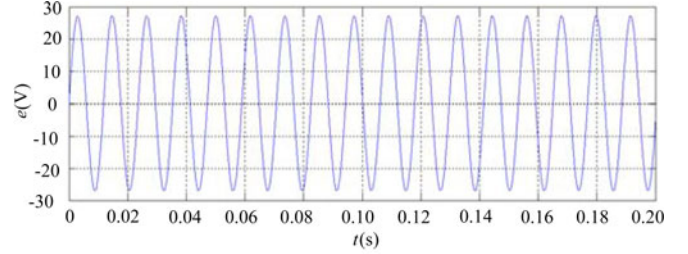


Fig. 8. Comparison of the pure integrator, the LPF, and the proposed algorithm: responses to the input EMF signal with an initial phase angle.

- 1) The dc gain of the pure integrator is  $\infty$  while that of the proposed algorithm is 0, which indicates that the dc drift problem associated with the pure integrator can be completely avoided by the proposed algorithm.
- 2) The amplitude- and phase-frequency characteristics of this proposed integration algorithm are same as those of the pure integrator at any synchronous angular frequency.
- 3) The fifth-order LPF in the proposed integration algorithm can effectively filter out HF harmonics in the back EMF.

The proposed integration algorithm is suitable for use in high-performance motor drives. The DTC scheme for EEFS generator dc power system is such a case that stator flux linkage has to be estimated with a high accuracy.

#### IV. SIMULATION

The performance of the proposed integration algorithm for stator flux estimation is investigated by MATLAB/Simulink.

Fig. 8 shows the stator back EMF at initial phase angle of  $90^\circ$  and the estimated flux linkages using the pure integrator, the LPF, and the proposed integration algorithm, respectively. As can be seen, a constant dc offset appears at the output of the integrator due to the initial value problem, the LPF produces errors both in phase angle and in magnitude, and the output of the proposed algorithm is coincident with the actual motor

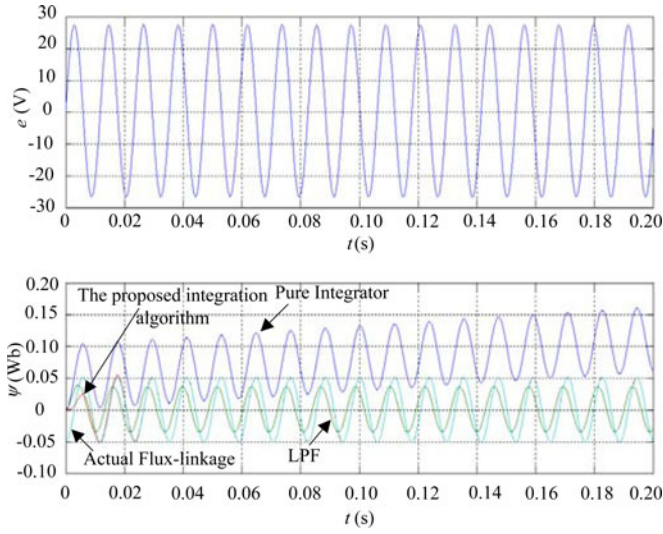


Fig. 9. Comparison of the pure integrator, the LPF, and the proposed algorithm: responses to the input EMF signal with a dc bias.

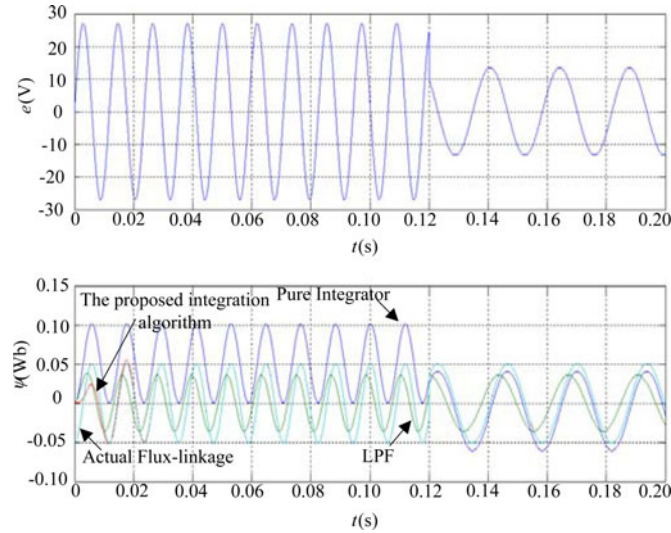


Fig. 10. Comparison of the pure integrator, the LPF, and the proposed algorithm: responses to a step change of the input EMF.

flux linkage, which demonstrate that the initial value problem is completely avoided by the proposed algorithm.

To investigate the dc drift problem, a dc bias is superimposed to sinusoidal back EMF inputs. Fig. 9 shows the estimated flux linkages using the three methods, respectively. It can be observed that the flux linkage estimated by the pure integrator has a slope bias and will finally be driven into saturation, and that by the LPF has phase angle and magnitude errors, whereas that by the proposed integration algorithm has no errors in the magnitude and phase angle and, the dc bias can be completely eliminated.

Fig. 10 shows the estimated flux linkages using the three methods to a step change in the back EMF. As can be seen, the pure integrator has undesired dc offsets all the time and the LPF brings phase angle and magnitude errors, whereas there is no dc offset in the flux-linkage waveform of the proposed algorithm.

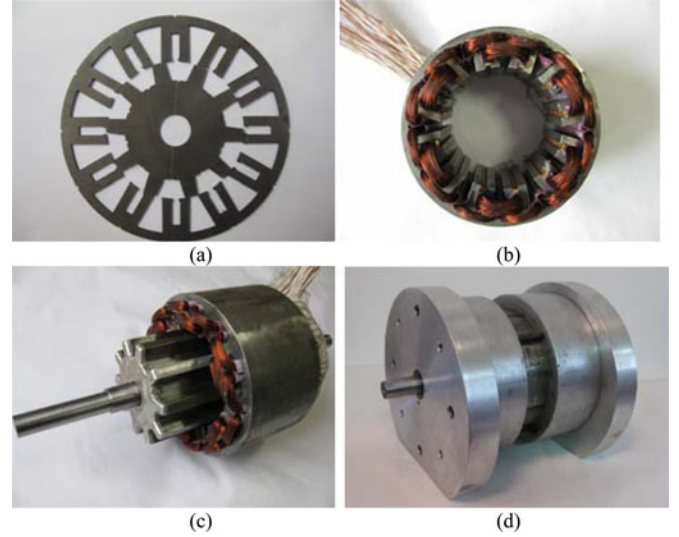


Fig. 11. Prototype machine.

TABLE III  
MACHINE DIMENSIONS AND PARAMETERS

Quantity	
Stator pole number	12
Rotor pole number	10
Stator outer diameter	150mm
Rotor outer diameter	89mm
Active axial length	100mm
Air-gap length	0.5mm
Split ratio	0.6
Rotor pole width	10.5°
Rated power	4.7kw
Rated torque	15Nm
Rated speed	3000rpm
Rated stator flux linkage	0.0496Wb

## V. EXPERIMENTAL RESULTS

To verify the proposed integration algorithm for stator flux estimation, the DTC scheme using the proposed algorithm is implemented on an EEFS generator dc power system and experimental tests have been carried out. Fig. 11 shows the prototype machine and the machine dimensions and parameters are shown in Table III.

The phase currents  $i_a, i_b, i_c$  are acquired by current sensors LA28-NP and phase voltages  $u_a, u_b, u_c$  are acquired as follows [10]:

$$\begin{aligned}
 u_a &= \frac{u_{dc}}{3} (2D_A - D_B - D_C) \\
 u_b &= \frac{u_{dc}}{3} (2D_B - D_A - D_C) \\
 u_c &= \frac{u_{dc}}{3} (2D_C - D_A - D_B)
 \end{aligned} \quad (21)$$

where  $D_A, D_B,$  and  $D_C$  are the duty ratios of leg A, leg B, and leg C, respectively, and the dc bus voltage  $u_{dc}$  is acquired by a voltage sensor LV28-P.

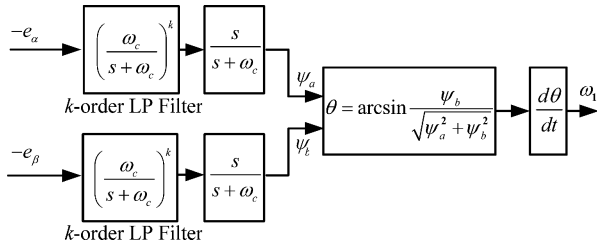


Fig. 12. Estimation of the generator synchronous angular frequency  $\omega_1$ .

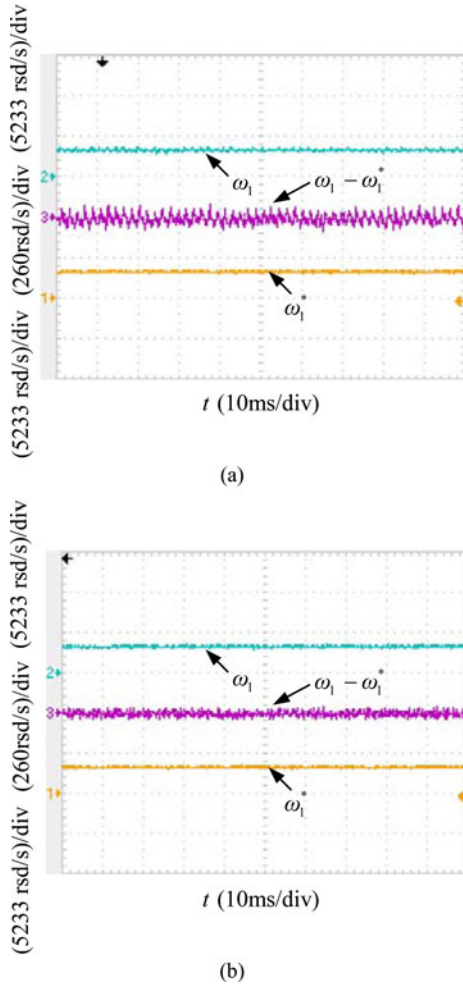


Fig. 13. Estimated  $\omega_1$  and the measured  $\omega_1^*$ . (a)  $\omega_c = 50$  rad/s;  $k = 2$ . (b)  $\omega_c = 5$  rad/s;  $k = 4$ .

The synchronous angular frequency  $\omega_1$  is estimated through a  $k$ -order LPF, an arcsine part, and a differential operation part, as shown in Fig. 12.

At 3000 r/min ( $\omega_1 = 3140$  rad/s), Fig. 13 shows the estimated synchronous angular frequency  $\omega_1$  using the method in Fig. 12 and the measured synchronous angular frequency  $\omega_1^*$  by a speed sensor (NOC-S5000-2MD). In Fig. 13(a), the peak value of estimated errors ( $\omega_1 - \omega_1^*$ ) is 102 rad/s, while in Fig. 13(b), it is 53 rad/s. It can be found that smaller  $\omega_c$  and higher  $k$  can improve the estimation accuracy of  $\omega_1$ .

The estimated stator flux linkages using the integration algorithm are shown in Fig. 14, where  $\psi_{\alpha(1)}$  is the estimated stator

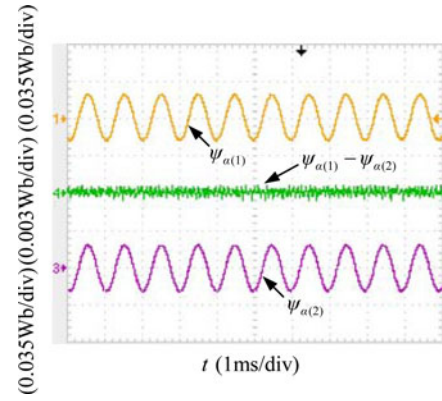


Fig. 14. Estimated stator flux linkages.

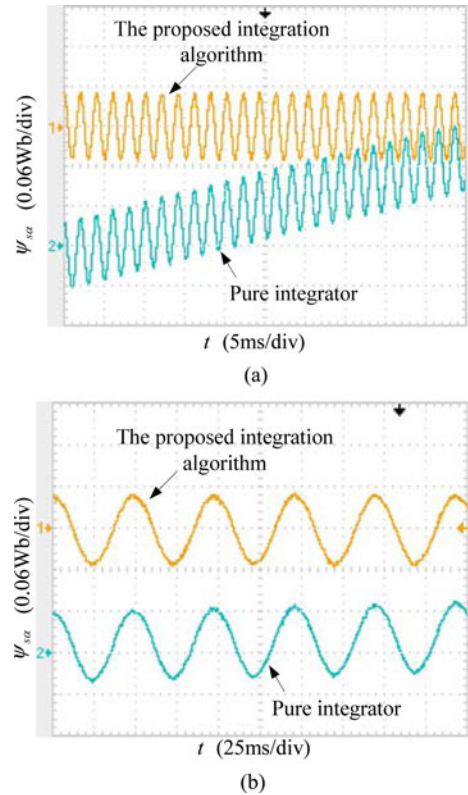


Fig. 15. Estimated stator flux linkages using the proposed integration algorithm and the pure integrator: (a) at 3000 r/min (b) at 120 r/min.

flux linkage based on the estimated synchronous angular frequency  $\omega_1$ , and  $\psi_{\alpha(2)}$  is that based on the measured one  $\omega_1^*$ . The peak value of  $\psi_{\alpha(1)} - \psi_{\alpha(2)}$  is 0.0006 Wb, which is only 2.4% of the stator flux-linkage magnitude. It can be found that  $\omega_1$  of high accuracy can guarantee the correctness of the integration process in terms of both amplitude and phase.

#### A. Steady-State Performance

At the rated speed, Fig. 15(a) shows the estimated stator flux linkages using the pure integrator and the proposed integration algorithm, respectively. The results at 120 r/min are also given, as shown in Fig. 15(b). It can be observed that the output of the

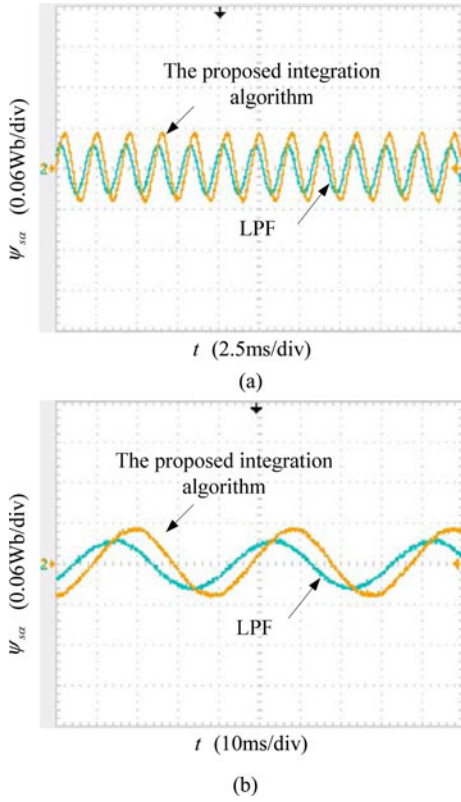


Fig. 16. Estimated stator flux linkages using the proposed integration algorithm and the LPF: (a) at 3000 r/min (b) at 150 r/min.

pure integrator diverges, whereas that of the proposed algorithm is a stable sine wave with no dc offset.

Fig. 16(a) shows the estimated stator flux linkages using the LPF and the proposed integration algorithm, respectively. Fig. 16(b) gives the results at 150 r/min. It can be found that the output of the LPF has magnitude reduction and phase lag.

Fig. 17 shows the output voltage and the electromagnetic torque of the DTC scheme at 50% of the rated load and the rated load, respectively. It can be seen that under different load conditions, the high-accuracy stator flux linkage estimated by the proposed algorithm can always maintain the output voltage stable.

From the previous analysis, it can be found that under different speed or load conditions, the proposed algorithm can well estimated the stator flux linkage, and thus improve the system performance.

Figs. 18 and 19 show the stator flux linkages and output voltage at 85 and 170 r/min, respectively.

Fig. 20 shows the stator flux linkage and output voltage when the speed varies slowly from 85 to 170 r/min (the reversing time is 16 s).

Based on previous results, it can be found that the integration algorithm behaves well at the low-speed region under loaded machine, which can guarantee the output voltage stable.

**B. Dynamic Performance**

Fig. 21 gives experimental results when 40% of the rated load is suddenly removed and applied. When 40% of the rated load is

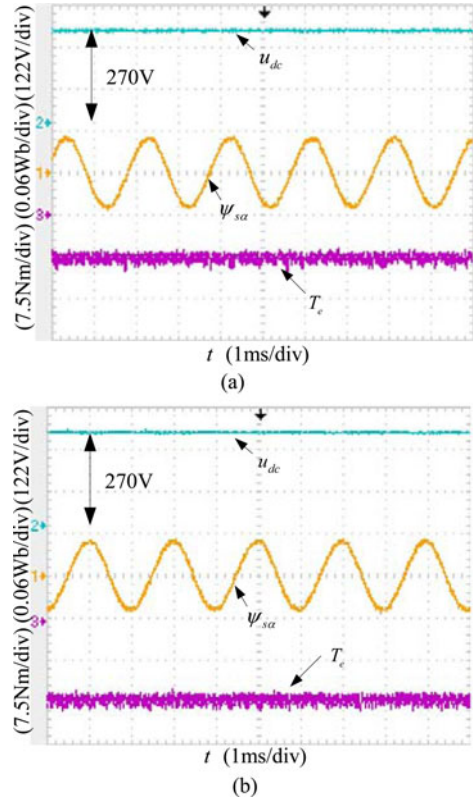


Fig. 17. Output voltage and torque at: (a) 50% of the rated load (b) the rated load.

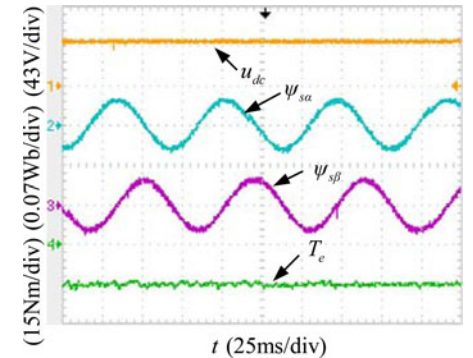


Fig. 18. Stator flux linkages and output voltage at 85 r/min ( $T_e = 15$  N·m).

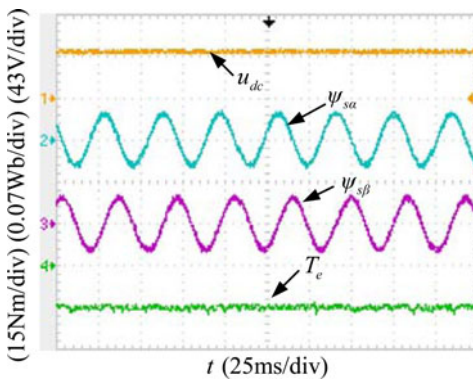


Fig. 19. Stator flux linkages and output voltage at 170 r/min ( $T_e = 15$  N·m).

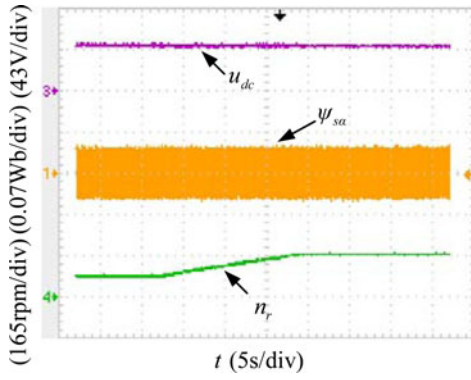


Fig. 20. Output voltage when the speed varies from 85 to 170 r/min.

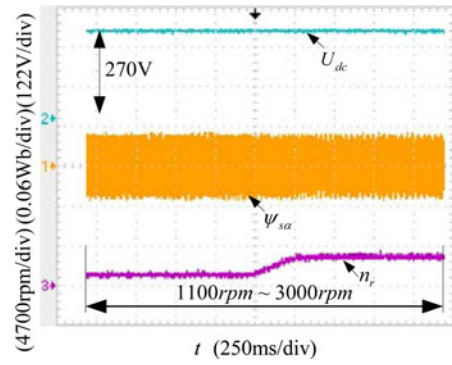
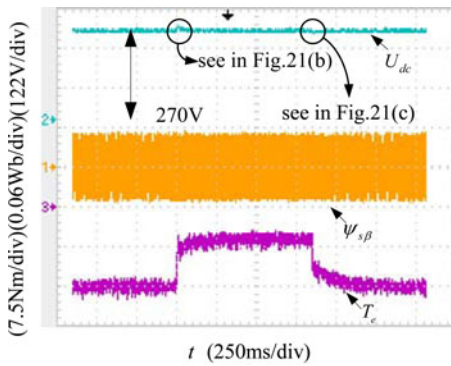
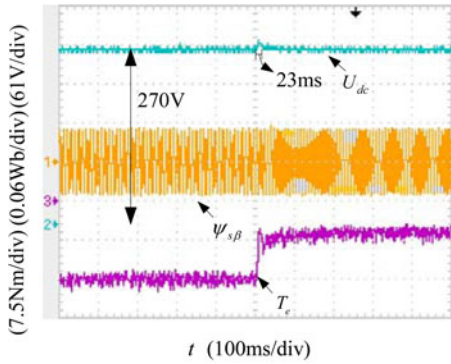


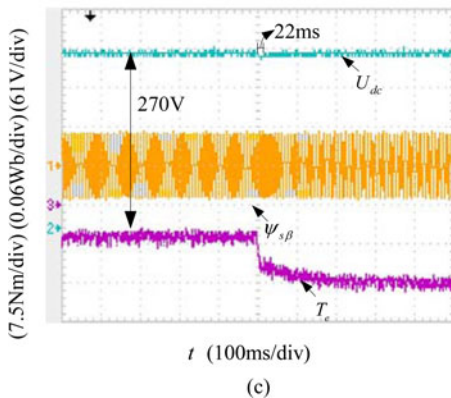
Fig. 22. Output voltage when the speed varies from 1100 to 3000 r/min.



(a)



(b)



(c)

Fig. 21. Results of load step changes: (a) 40% of the rated load is suddenly removed and applied; (b) blow up of (a) when the load is suddenly removed; (c) blow up of (a) when the load is suddenly applied.

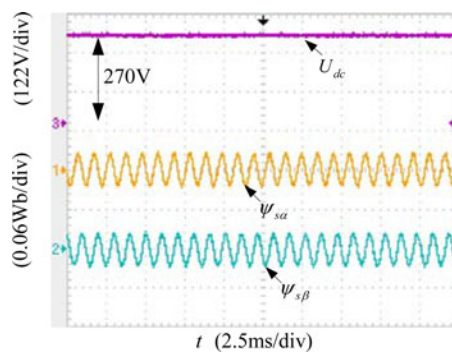


Fig. 23. Output voltage and stator flux linkages at 6000 r/min.

suddenly removed, the voltage recovery time is only 23 ms, as shown in Fig. 21(b). The recovery time when the load is applied is only 22 ms, as shown in Fig. 21(c). It can be found that the estimated stator flux linkage using the proposed algorithm can make accurate selection of voltage vectors to rapidly change the torque and thus achieve high system dynamic performance.

Fig. 22 gives experimental results when the speed varies from 1100 to 3000 r/min. It can be seen that under speed change condition, the stator flux linkage estimated by the proposed algorithm can guarantee output voltage stable.

### C. Flux Weakening Region

Fig. 23 gives the output voltage and stator flux linkages at 6000 r/min. Fig. 24(a) and (b) gives stator flux-linkage vector trajectory in the constant torque region (at 3000 r/min) and the flux weakening region (at 6000 r/min), respectively. It can be seen that at 6000 r/min, the magnitude of stator flux linkage is 0.248 Wb, which is 50% of the rated value.

Fig. 25 gives experimental results when the speed varies from 3000 to 6000 r/min. It can be seen that when the speed changes, the estimated stator flux-linkage magnitude can rapidly response to the change of the reference value, which can guarantee the output voltage stable in wide speed range.

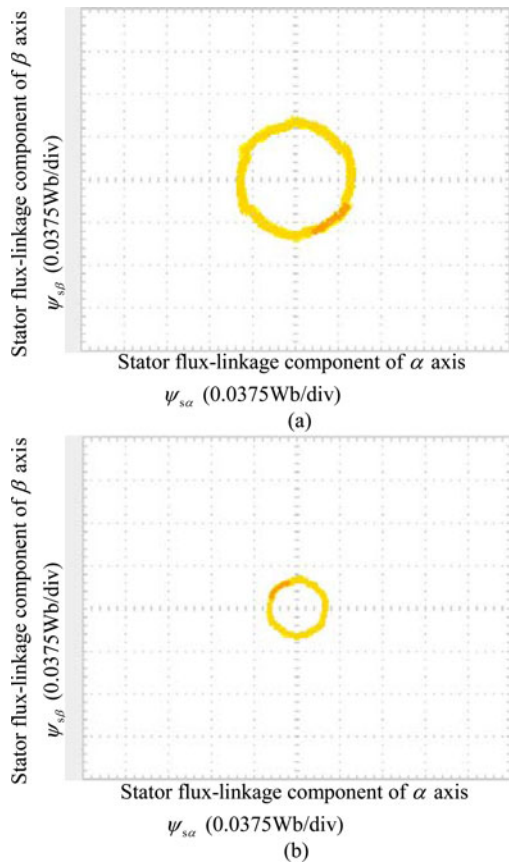


Fig. 24. Stator flux-linkage vector trajectory: (a) at 3000 r/min (b) at 6000 r/min.

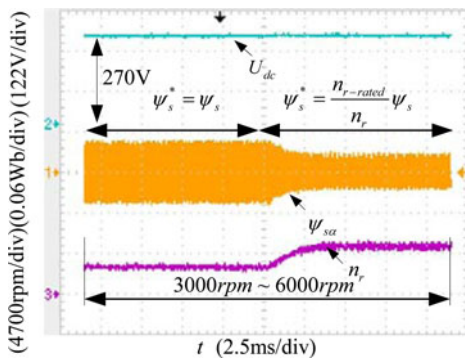


Fig. 25. Output voltage when the speed varies from 3000 to 6000 r/min.

## VI. CONCLUSION

An integration algorithm for stator flux estimation, which consists of a fifth-order filter, an HP filter, and a logical calculation part, is investigated for the DTC scheme of EEFS generator. The combination of the three parts in this algorithm can not only effectively solve the problems associated with the LPF, but also achieve same amplitude- and phase-frequency characteristics as those of the pure integrator at any synchronous angular frequency, and meanwhile the dc gain is zero.

The DTC using the proposed algorithm for EEFS generator dc power system is implemented. The experimental results demonstrate that the proposed integration algorithm exhibits

good estimation capability in both steady state and dynamic conditions, and thus improves the system quality.

Furthermore, this simple and practical integration algorithm is also suitable for other high-performance BLac machine drives, such as stator flux field-oriented control and DTC of induction machines and flux-switching permanent magnet machines.

## REFERENCES

- [1] Y. Hu, W. Huang, and Y. Li, "A novel instantaneous torque control scheme for induction generator systems," *IEEE Trans. Energy Convers.*, vol. 25, no. 3, pp. 795–803, Sep. 2010.
- [2] A. K. Jain, S. Mathapati, V. T. Ranganathan, and V. Narayanan, "Integrated starter generator for 42-V power net using induction machine and direct torque control technique," *IEEE Trans. Power Electron.*, vol. 21, no. 3, pp. 701–710, May 2006.
- [3] L. Xu and P. Cartwright, "Direct active and reactive power control of DFIG for wind energy generation," *IEEE Trans. Energy Convers.*, vol. 21, no. 3, pp. 750–758, Aug. 2006.
- [4] G.-D. Andreescu, C. I. Pitic, F. Blaabjerg, and I. Boldea, "Combined flux observer with signal injection enhancement for wide speed range sensorless direct torque control of IPMSM drives," *IEEE Trans. Energy Convers.*, vol. 23, no. 2, pp. 393–402, Jun. 2008.
- [5] N. R. N. Idris and A. H. M. Yatim, "An improved stator flux estimation in steady-state operation for direct torque control of induction machines," *IEEE Trans. Ind. Appl.*, vol. 38, no. 1, pp. 110–116, Jan./Feb. 2002.
- [6] R. Wu and G. R. Slemon, "A permanent magnet motor drive without a shaft sensors," *IEEE Trans. Ind. Appl.*, vol. 27, no. 5, pp. 1005–1011, Sep. 1991.
- [7] J. Hu and B. Wu, "Improved integration algorithms for estimating motor flux over a wide speed range," *IEEE Trans. Power Electron.*, vol. 13, no. 5, pp. 969–977, Sep. 1998.
- [8] P. Vas, *Sensorless Vector and Direct Torque Control*. London, U.K.: Oxford Science Publication, 1998.
- [9] K. Rajashekar, A. Kawamura, and K. Matsuse, *Sensorless Control of AC Motor Drives*. New York: IEEE Press, 1996.
- [10] M.-H. Shin, D.-S. Hyun, S.-B. Cho, and S.-Y. Choe, "An improved stator flux estimation for speed sensorless stator flux orientation control of induction motors," *IEEE Trans. Power Electron.*, vol. 15, no. 2, pp. 312–318, Mar. 2000.
- [11] M. Cirrincione, M. Pucci, G. Cirrincione, and G. A. Capolino, "A improved adaptive integration methodology for estimating flux in induction machine drives," *IEEE Trans. Power Electron.*, vol. 19, no. 1, pp. 25–34, Jan. 2004.
- [12] J. Holtz and J. Quan, "Sensorless vector control of induction motors at very low speed using a nonlinear inverter model and parameter identification," *IEEE Trans. Ind. Appl.*, vol. 38, no. 4, pp. 1087–1095, Jul./Aug. 2002.
- [13] J. Holtz and J. Quan, "Drift- and parameter-compensated flux estimator for persistent zero-stator-frequency operation of sensorless-controlled induction motors," *IEEE Trans. Ind. Appl.*, vol. 39, no. 4, pp. 1052–1060, Jul./Aug. 2003.
- [14] Z. Q. Zhu and J. T. Chen, "Advanced flux-switching permanent magnet brushless machine," *IEEE Trans. Magn.*, vol. 46, no. 6, pp. 1447–1452, Jun. 2010.
- [15] J. T. Chen, Z. Q. Zhu, S. Iwasaki, and R. Deodhar, "Low cost flux-switching brushless AC machines," in *Proc. IEEE Vehicle Power Propulsion Conf.*, Sep. 2010, pp. 1–6.
- [16] C. Lascu, I. Boldea, and F. Blaabjerg, "Direct torque control of sensorless induction motor drives: A sliding-mode approach," *IEEE Trans. Ind. Appl.*, vol. 40, no. 2, pp. 582–590, Mar./Apr. 2004.
- [17] Z. Q. Zhu, Y. Liu, and D. Howe, "Minimizing the influence of cogging torque on vibration of PM brushless machines by direct torque control," *IEEE Trans. Magn.*, vol. 42, no. 10, pp. 3512–3514, Oct. 2006.
- [18] Y. Liu, Z. Q. Zhu, and D. Howe, "Commutation-torque-ripple minimization in direct-torque-controlled PM brushless DC drives," *IEEE Trans. Magn.*, vol. 43, no. 4, pp. 1012–1021, Jul./Aug. 2007.
- [19] Y. Hu, L. Zhang, W. Huang, and F. Bu, "A fault-tolerant induction generator system based on instantaneous torque control (ITC)," *IEEE Trans. Energy Convers.*, vol. 25, no. 2, pp. 412–421, Jun. 2010.
- [20] I. Boldea, L. Janosi, and F. Blaabjerg, "A modified direct torque control (DTC) of reluctance synchronous motor sensorless drive," *Electr. Machines Power Syst.*, vol. 28, no. 2, pp. 115–128, Feb. 2000.



**Yu Wang** (A'12) received the B.Eng. and M.Sc. degrees in electrical engineering from the Nanjing University of Aeronautics and Astronautics, Nanjing, China, in 2004 and 2007, respectively, where he is currently working toward the Ph.D. degree in the Department of Electrical Engineering.

He is the holder of 10 China Invention Patents. His research interests include design and control of flux-switching machines.



**Zhiquan Deng** was born in Hubei, China, in 1969. He received the B.S. degree in mechanical engineering from Xi'an Institute of Metallurgy and Construction Engineering (which has been known as Xi'an University of Architecture and Technology since 1994), Xi'an, China, in 1990, and the M.S. and Ph.D. degrees in engineering machinery from Northeastern University, Liaoning, China, in 1993 and 1996, respectively.

In 1996, he was a Postdoctoral Fellow at the Nanjing University of Aeronautics and Astronautics, Nanjing, China, where he joined the Department of Electrical Engineering in 1998 and is currently a Professor at the College of Automation Engineering. His current research interests include bearingless motor drive systems, magnetic bearings, superhigh-speed electrical machines, and flux-switching machines.